JOURNAL OF SPACECRAFT AND ROCKETS
Vol. 45, No. 3, May–June 2008

Magnetohydrodynamics Interaction Over an Axisymmetric Body in a Hypersonic Flow

Andrea Cristofolini,* Carlo A. Borghi,* and Gabriele Neretti†
University of Bologna, I-40136 Bologna, Italy
Andrea Passaro‡ and Gabriele Fantoni§
Alta Società per Azioni, I-56014 Ospedaletto (PI), Italy
and
Fabrizio Paganucci¶
University of Pisa, I-56100 Pisa, Italy

DOI: 10.2514/1.29919

The magnetohydrodynamics interaction around a conical test body in a hypersonic argon flow is experimentally investigated. The hypersonic flow is realized in the high-enthalpy arc-heated wind tunnel of Alta Società per Azioni (S.p.A.) (Pisa, Italy) at Mach 6. The aim of experimental activity is to produce an experimental data base to be used for the validation of numerical codes for the analysis of the magnetohydrodynamics interaction. The magnetohydrodynamics interaction is obtained in the shock layer of the conical test body at the exit of the hypersonic nozzle. The electrical configuration realized allows one to enhance the effect of the magnetohydrodynamics interaction on the plasma parameters. This is done using the Hall field to generate the magnetohydrodynamics interaction and by short-circuiting the Faraday current inside the plasma of the shock layer. The magnetic flux density is produced by an array of three magnets located in the test body. Tests are performed at three different stagnation pressures. Fluid-dynamic, electrical, and optical observations have been done. The experiment showed a considerable effect of the magnetohydrodynamics interaction on the values of the quantities measured.

Nomenclature

$\mathbf{B}$	=	magnetic flux density
B	=	magnetic flux density modulus
B_i	=	magnetic flux density component along the i direction
Cp	=	pressure coefficient
$\mathbf{E}$	=	electric field
E_i	=	electric field component along the i direction
$\mathbf{J}$	=	electric current density
J_i	=	electric current density component along the i direction
p	=	pressure
$\mathbf{u}$	=	flow velocity
β_e	=	electron Hall parameter
μ_e	=	electron mobility
ρ	=	mass density
$\boldsymbol{\sigma}$	=	electrical conductivity tensor
σ	=	scalar electrical conductivity
φ	=	electric potential

Subscripts

mhd	=	measurement performed when the MHD interaction is active
nm	=	measurement performed when the MHD interaction is not active
r, z, θ	=	directions in a cylindrical coordinate system
∞	=	freestream condition

Presented as Paper 8008 at the 14th AIAA/AHI Space Planes and Hypersonic Systems and Technologies Conference, Canberra, 6–9 November 2006; received 22 January 2007; accepted for publication 2 May 2007.

*Professor, Department of Electrical Engineering, Viale Risorgimento 2. Member AIAA.
†Ph.D. Student, Department of Electrical Engineering, Viale Risorgimento 2. Student Member AIAA.
‡Project Manager, Via Gherardesca 5. Member AIAA.
§Project Engineer, Via Gherardesca 5.
¶Professor, Department of Aerospace Engineering, Via Diotisalvi 2. Member AIAA.

I. Introduction

IN THE past, several studies on the magnetohydrodynamics (MHD) interaction in hypersonic flows for aerospace applications have been done [1–8]. Considerable effort has been devoted to create the physical models and the numerical coding for the analyses of the MHD interaction in hypersonic flows [9–11]. Various experiments on MHD interaction have been carried out in laboratory test facilities [12–14]. Blunt and sharp configurations have been investigated [15] to explore the appealing opportunity to control an ionized gas flow by means of an electromagnetic body force. Remarkable work has been carried out to develop and to improve nonintrusive measurement techniques for a correct evaluation of the effects of the MHD interaction [16]. However, due to the difficulties of reproducing the MHD interaction in a well-characterized plasma flow, experimental activities are few and often yield results that cannot be readily used to validate the numerical codes.

The typical working conditions for MHD experiments in a hypersonic regime are characterized by low pressure plasmas. In this condition, which is also found during the reentry phase of a hypersonic vehicle in a planetary atmosphere, the plasma is characterized by relatively high values of the electron mobility and, thus, of the Hall parameter. This means that the electric current density will exhibit some tendency to flow in a perpendicular direction to the magnetic flux density and to the electric force per charge unit $E + U \times B$. This feature, if not properly dealt with, can significantly spoil the effect of the MHD interaction. An effective approach would be to use a Hall configuration, that is to exploit the Hall component (i.e., the component parallel to the flow velocity) of the electric field to sustain the current density which generates MHD

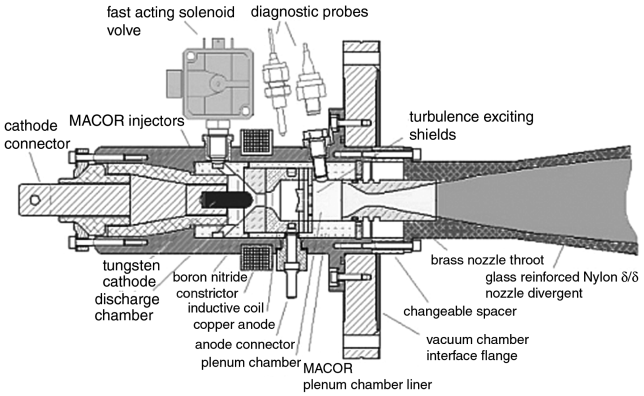

Fig. 1 Arc heater scheme.

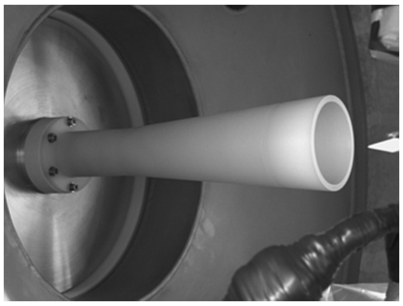

Fig. 2 The nozzle mounted at the exit of the settling chamber.

interaction. This can be done by shorting the Faraday field (i.e., the electric field component in the $U \times B$ direction).

In recent work [17], the experimental results of the MHD interaction in a hypersonic regime on a test body with a Hall electrodynamic configuration have been presented. The magnetic configuration was designed to maximize the effect of the MHD interaction in a high Hall parameter plasma. The magnetic flux density was perpendicular to the test body surface, and a set of electrodes was positioned on the test body surface to short the Faraday field. However, despite the electrodes configuration, the measured electric potential on the test body surface revealed that the Faraday component of the electric field was not shorted. The proposed explanation was that the boundary layer, constituted by a low electrical conductivity plasma, introduces a high electric resistance for the current between the test body and the core flow and prevents the shorting of the Faraday field, hence causing a reduction of the effect of the MHD interaction.

In this paper, the results of a new experimental activity on MHD interaction in hypersonic flow are presented. The experiment is expressly designed to generate results to be used for the validation of numerical codes. A conical geometry, which was previously proposed and numerically investigated [18] is used for the test body. This configuration allows one to implicitly short the Faraday component of the electric field and produces truly two-dimensional results for numerical validation. The magnetic flux density is produced by an array of permanent magnets. Argon is used as a working gas.

The configuration can be considered as the first necessary step toward the model and code validation as well as the first tentative step of utilization of the MHD interaction in real hypersonic applications. Although the sharp cone can be considered as an extremely simplified model of an advanced vehicle nose, the experimental activity described in this paper offers basic knowledge of the MHD interaction and insight into the physical phenomena involved. The information gathered from this work will be useful for the development of further activities, with the next goal being the mitigation of the incoming heat flux on a blunt body configuration, which provides a significant challenge due to the modification of the flowfield conditions in this case.

II. Experimental Setup

An Alta high-enthalpy arc-heated tunnel (HEAT) is a pulsed hypersonic wind tunnel operative since 1996 [19,20]. It can produce Mach 6 flows in a low to medium Reynolds number range (10^4–10^6). In the wind-tunnel settling chamber the gas is heated by means of an arc discharge powered by a 260 kW dc power supply and delivering arc currents up to 630 A during running times of 20–300 ms. In the settling chamber a total specific enthalpy up to 6 MJ/kg with stagnation pressures up to 9 bar can be obtained. The gas heater can be operated with air, nitrogen, argon, and CO_2 in a pulsed, quasi-steady mode. At the exit of the settling chamber a nozzle is mounted. The effective test section at the exit of the nozzle has a diameter of 45 mm. The arc heater scheme is shown in Fig. 1. The nozzle is shown in Fig. 2. The wind tunnel (gas heater and nozzle) is installed on a vacuum test section of 600 mm in diameter. In the test section there are optical accesses from all sides. This section is connected to a vacuum chamber of a volume of 4.1 m^3. The chamber is evacuated by four rotary pumps to reach an ultimate pressure of 10 Pa before each run. The flow characteristics are obtained by means of pitot probes provided with fast miniaturized piezoresistive pressure transducers and stagnation temperature probes provided with fast coaxial thermocouples or thin-film gauges. In the settling chamber the pressure is measured by fast pressure transducers. Accuracies of about 3% are obtained in all pressure measurements. The total enthalpy is evaluated from the arc discharge power and compared with the values obtained from the stagnation temperature measured in the test section. The total enthalpy error is ±5–10%.

The test gas used in this experiment is argon. A short Mach 6 conical nozzle with an effective exit test section of a diameter of about 50 mm is used. A series of preliminary tests allowed one to identify the best conditions for the arc discharge. The arc voltage was between 55 and 65 V for all test conditions. Three typical test conditions with a pressure in the plenum chamber (plenum pressure) ranging between 0.5 and 0.7 bar are considered. Pressure fluctuations are observed at pressures below 0.5 bar. This is due to the turbulence created in the settling chamber. The three test conditions are reported in Table 1. Here the values of the Mach number, the mass flow rate, the stagnation pressure, and the stagnation temperature are reported. The stagnation pressure and the stagnation temperature are given by the pressure measured in the plenum chamber. Because of the relatively high variance of the flow conditions during the hot runs (about 15%), at each gas condition of Table 1 the runs were repeated from 5 to 10 times and average values of the signals were considered.

Properties such as electron temperature and electron density are required for the evaluation of the electric transport properties of the plasma (i.e., electron mobility and electrical conductivity), which are essential data for the numerical rebuilding of the experiment and for the interpretation of the experimental results. Thus, a crucial point is the evaluation of the plasma parameters in the freestream flux at the nozzle exit. In order to do this, optical diagnostics and microwave

Table 1 Flow characteristics for the test conditions

Condition	Mach no.	Mass flow rate, g/s	Arc voltage, V	Arc current, A	Stagnation pressure, mbar	Stagnation temperature, K	Electron density ($\times 10^{18}$), m^{-3}	Electron temperature, eV
1	6.16	4.46	55.30	518.5	523	4455.7	75.11	0.216
2	6.19	5.34	58.61	509.4	589	3850.4	58.4	0.221
3	6.10	7.027	64.55	520.0	653	3344.2	24.68	0.227

measurements have been used and the results have been reported [21]. The flow characterization in the plenum chamber and at the exit of the nozzle is also taken from [21]. Three typical test conditions are identified with a total pressure ranging between 0.5 and 0.7 bar and are summarized in Table 1.

As described in the previously mentioned paper [21], the electron number density and temperature have been experimentally evaluated in the plenum chamber. These results have been then used as input for a numerical model [22], which solves the quasi-two-dimensional steady Euler equations for the nozzle expansion. The model is coupled with the state-to-state kinetics, and the internal state kinetics is coupled with the Boltzmann equation for free electrons. The two last columns of Table 1 report the electron number density and temperature at the exit of the nozzle resulting from calculations.

The diagnostic results reported in this paper are from pressure measurements and electric voltage measurements in the shock layer of the test body and imaging of the plasma under the MHD interacting effect. A PCO SensiCam 1280 × 1024 interline charge-coupled device (CCD) color camera, with a minimum exposure time of 100 ns, has been used for the imaging of the MHD interacting plasma. The CCD quantum efficiency peak is nearly 53% at a wavelength of 380 nm. The electric measurements are done by means of two sets of five electrical probes mounted on the test body wall. To perform the pressure measurements a single miniaturized Kulite fast pressure transducer (model XCS-062-5A) was mounted flush with the wall, halfway along the lateral surface of the test body. Because of the expected low level of the pressure to be measured, the pressure signal was sent to an amplifier circuit based on the Analog Devices SSM2019 chips, which allows ×10, ×100, and ×1000 dc gain. The signals were acquired through the HEAT data acquisition (DAQ) system, based on the Labview 7 environment and a National Instruments 6071 board.

III. Test Body Design

At the low plasma densities, typical of the reentry of hypersonic vehicles into the atmosphere, the Hall parameter is high. The test body design is thus aimed to exploit the Hall field in sustaining the Faraday current which generates the MHD interaction. To do this, a conical geometry with the axis of the cone directed along the gas freestream flow is chosen.

In the frame of the low magnetic Reynolds number approximation [23], the curl free electric field $\mathbf{E}$, and the current density are

$$\mathbf{E} = -\nabla\varphi, \qquad \nabla\cdot\mathbf{J} = 0 \tag{1}$$

Ohm's law is given by

$$\mathbf{J} = \boldsymbol{\sigma}(\mathbf{E} + \mathbf{u}\times\mathbf{B}) \tag{2}$$

where the conductivity tensor $\boldsymbol{\sigma}$, in the two-dimensional geometry of a reference system, and where the gas velocity $\mathbf{u}$ and the magnetic flux density $\mathbf{B}$ lie on the r–z plane and the electromotive force $\mathbf{u}\times\mathbf{B}$ is directed along the φ axis, has the following expression [23]:

$$\boldsymbol{\sigma} = \frac{\sigma}{1+\beta_e^2}\begin{bmatrix} 1+\beta_z^2 & \beta_z\beta_r & \beta_r \\ \beta_z\beta_r & 1+\beta_r^2 & -\beta_z \\ -\beta_r & \beta_z & 1 \end{bmatrix}$$

with

$$\beta_z = B_z\frac{\beta_e}{B} = \mu_e B_z, \qquad \beta_r = B_r\frac{\beta_e}{B} = \mu_e B_r$$

To get insight into the electrodynamics in the proposed geometry, an annular channel may be considered (Fig. 3). Here the gas flow velocity $\mathbf{u}$ is in the z direction and the $\mathbf{B}$ field is in the r direction. Assuming that in the azimuthal direction the electric field component is short-circuited ($E_\varphi = 0$), Ohm's law becomes

$$j_z = \frac{\sigma}{1+\beta_e^2}(E_z + \beta_e uB) \qquad j_r = \beta E_r$$

$$j_\varphi = \frac{\sigma}{1+\beta_e^2}(-\beta_e E_z + uB)$$

Assuming that the current component in the r direction J_r is equal to zero, it is $E_r = 0$ (when the two opposite walls perpendicular to the r direction are not electrically connected). As a consequence, the electric potential along the r direction is constant and is only a function of the z variable. The conservation of the magnetic flux depends on the radius and is $B_r(r) = B_0, r_0/r$. Assuming to keep the current flowing in the z direction equal to zero, it follows that

$$I_z = \int_{r_0}^{r_1} J_z r\,\mathrm{d}r \approx \sigma\int_{r_0}^{r_1}[(E_z + \beta_e uB)r/\beta_e^2]\,\mathrm{d}r = 0 \tag{3}$$

and

$$E_z = -2\mu_e u(B_0 r_0)^2/(r_0^2 + r_1^2) \tag{4}$$

From Eq. (4) the azimuthal component of the current density can be evaluated:

$$j_\varphi \approx 2\sigma u B_0 r_0 r/(r_0^2 + r_1^2) \tag{5}$$

Equation (5) shows that in the axial-symmetric geometry, the azimuthal component of the current density is not affected by a high Hall parameter when the current flowing in the z direction is kept equal to zero. Furthermore, Eq. (4) shows that for high electron mobility and high Hall parameters ($\beta_e = B\mu_e$), the Hall electric field can properly sustain the Faraday current density as given by Eq. (5).

The exposed analysis can be qualitatively applied to the experiment presented in this paper. The test body is placed at the exit of the nozzle with the axis of the cone in the direction of the gas flow. The shock layer around the test body can be regarded as the annular channel, confined between the wall of the test body and the shock front.

The magnetic flux density required for the MHD interaction is generated by means of an array of three permanent magnets as shown in Fig. 4. The magnetic flux density produced by this arrangement has been calculated by means of a magnetostatic finite element numerical code, and the results are shown in Fig. 4. The configuration adopted appears to be particularly suitable as it does not require any conductor carrying current for the generation of the magnetic flux density. The magnets have been arranged alternating the three conical permanent magnet sections with an ARMCO iron

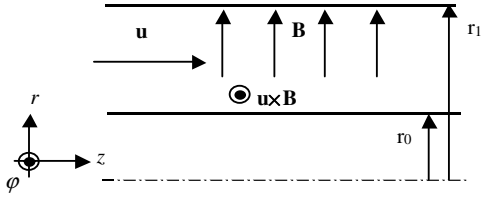

Fig. 3 The annular channel in an axial-symmetric geometry.

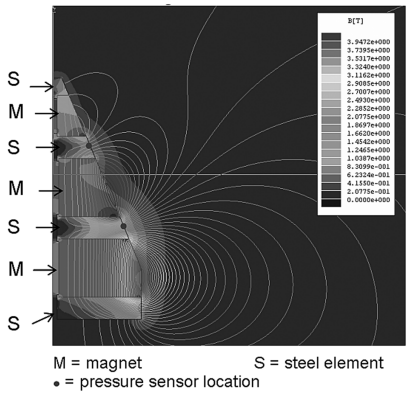

Fig. 4 The test body scheme and *B* field distribution.

Fig. 5 Test body assembly.

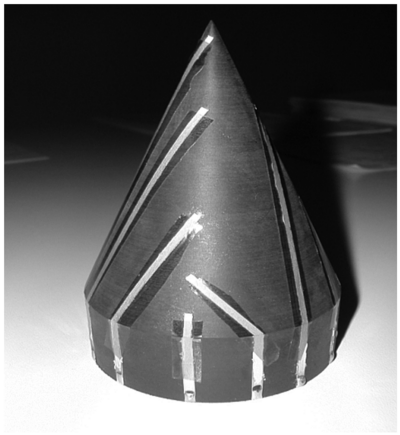

Fig. 6 The nylon shell, where the voltage probes are also visible.

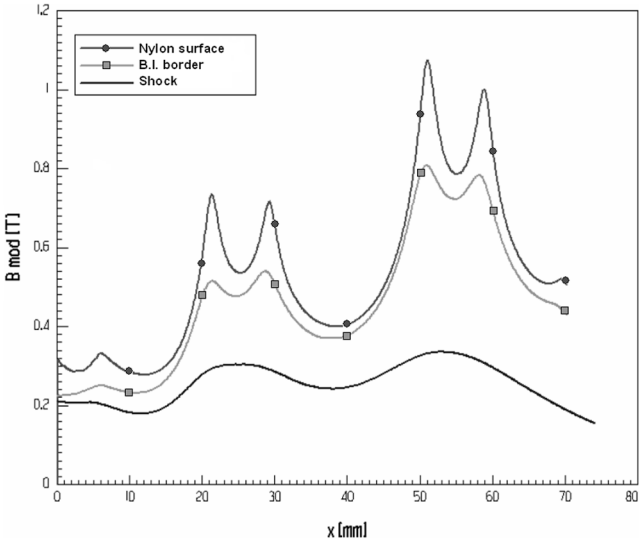

Fig. 7 Calculated *B* field modulus on the test body wall, on the border of the boundary layer region, and on the shock front surface.

section to form a cone with a half-vertex angle of 22.5 deg and a 60-mm base diameter. In Fig. 5, a picture of the assembled magnetic structure of the test body is shown. The magnetic structure is protected by a 1-mm thick conical shell of glass reinforced Nylon 6/6. A set of electrostatic probes for measuring the Hall field along the flux lines has been placed on the nylon shell, as shown in Fig. 6.

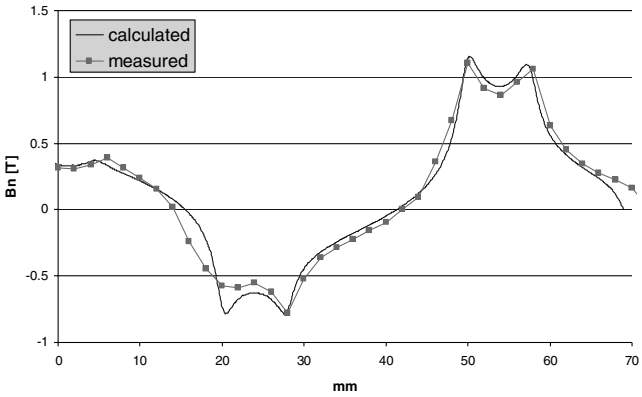

Fig. 8 Measured and calculated normal components of the magnetic flux density on the test body wall.

In Fig. 7, the calculated modulus of the magnetic flux density on three different lines is plotted: on the test body wall, 1 mm away from the test body wall (approximately at the border of the boundary layer region), and on the shock front, as resulting from the mentioned analysis. To validate the magnetostatic numerical results, Fig. 8 plots a comparison between the measured and calculated values of the normal component of the magnetic flux density on the test body wall.

A nonmagnetic conical test body with the same geometry has been built to evaluate the flow properties when the MHD interaction is not present. Both the test bodies were equipped with two miniaturized piezoresistive pressure sensors, located in the region where the most intense MHD interaction is expected.

IV. MHD Interaction Experiments

A. Pressure Measurements

In Figs. 9–13, the plots from pressure measurements are shown. All the plots are obtained from an ensemble average of the results from runs in the same operative condition. During the calibration runs it was seen how the transitory phase of pressure rise/decrease

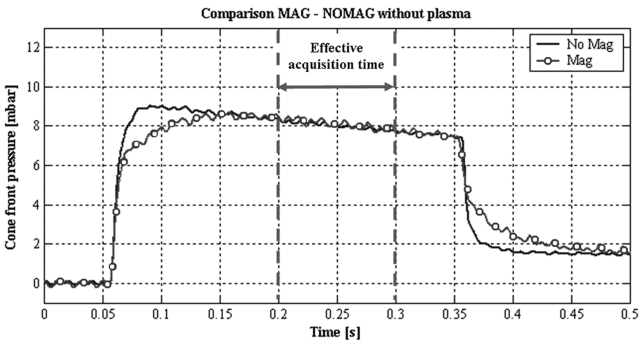

Fig. 9 Pressure behaviors with magnetic and nonmagnetic test bodies in cold conditions.

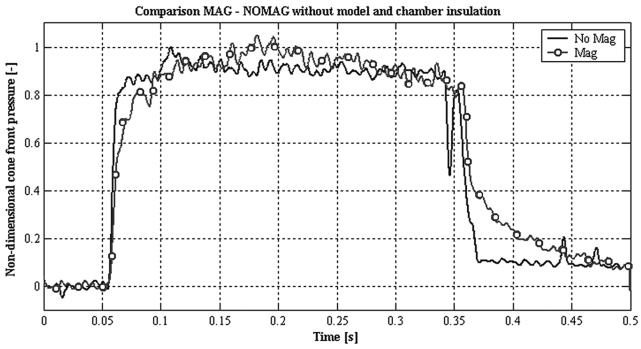

Fig. 10 Pressure behaviors with magnetic and nonmagnetic test bodies in a gas flow at condition 1 when the vacuum tank was not electrically insulated and the Hall field was short-circuited.

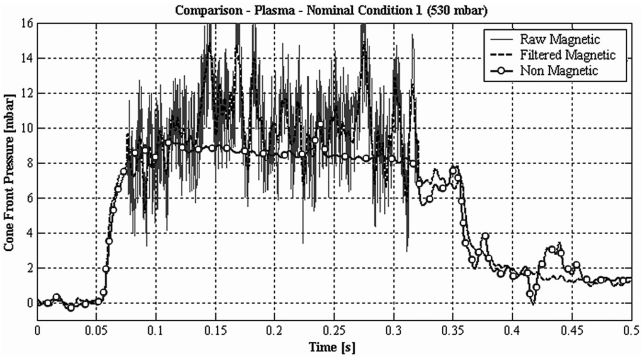

Fig. 11 Pressure measurements with and without MHD interaction at flow condition 1: the average pressure for the nonmagnetic case is 8.54 mbar, and for the MHD interaction case is 9.71 mbar (14% increase).

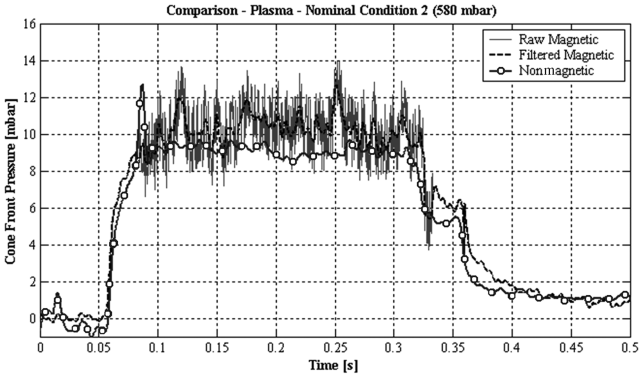

Fig. 12 Pressure measurements with and without MHD interaction at flow condition 2: the average pressure for the nonmagnetic case is 8.94 mbar, and for the MHD interaction case is 10.02 mbar (12% increase).

was different for the two test bodies (that were equipped with different sensors, but used the same external nylon shell), due to the minor geometrical differences between the two internal parts. Nonetheless, the signals were practically coincidental for more than 150 ms in the middle section of the run, starting approximately 100 ms after the valve pulse. For all of the runs, the pressure measurement was taken as the average value in the range between 200 and 300 ms from the acquisition start, that is, between 150 and 250 ms from the valve pulse (Fig. 9). Between 5 and 10 repetitions were carried out for each test condition and each model, to gather a statistically significant sample, given the relatively high variance of the flow total temperature in hot conditions (about 15%). Additionally, a careful cross calibration of the two model sensors was performed in cold and hot conditions at several pressure levels: in cold conditions the two models provide practically coincident results.

Pressure behaviors in time with magnetic and nonmagnetic test bodies are plotted in Fig. 10. The runs were done when the vacuum chamber wall was not electrically insulated and the Hall field was short-circuited through the tank, enabling possible closure patterns to the plasma currents. The two signals are nearly equal showing that

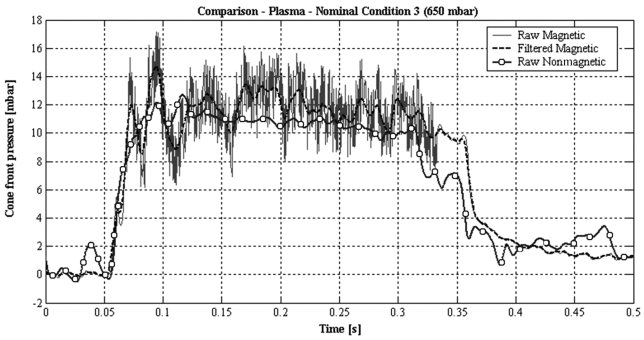

Fig. 13 Pressure measurements with and without MHD interaction at flow condition 3: the average pressure for the nonmagnetic case is 10.79 mbar, and for the MHD interaction case is 11.57 mbar (7% increase).

the MHD interaction is significantly spoiled by the short-circuiting of the Hall field. This is a strong indication of the importance of the Hall field in this experiment.

B. Test Results

The tests in the nominal configurations, that is, including model and chamber wall insulation, gave immediately interesting results: the nonmagnetic model presents a behavior perfectly comparable to the aforementioned calibration tests; the magnetic model pressure sensor, instead, provides an extremely noisy reading when the plasma is present, similar to a typically turbulent flow, and sometimes leading to a completely nonusable measurement due to DAQ board saturation. The comparison of the pressure with and without MHD interaction for conditions 1, 2, and 3 is shown in Figs. 11–13 respectively. The dashed lines in these figures are obtained by numerically filtering the pressure measurements in the MHD case. The freestream and the flow over the model should be completely laminar in all conditions, and, in fact, it appears laminar in all of the preliminary tests. The observed fluctuations with the magnetic test body are therefore probably generated by some form of interaction between the plasma and the magnetic field, although it is not clear what part of the signal is due to actual pressure fluctuations and what part is due to electromagnetic disturbances produced by plasma fluctuations. For this reason, for the "magnetic" runs, an ensemble average between all of the available runs was used to calculate the average pressure, leading to a relatively high variance in the obtained value (typical variance in the nonmagnetic runs is well below 2%, while it is of about 5–10% in the magnetic ones).

For all of the test conditions, an increase of the average pressure is recorded with the magnetic test body, with the highest increase corresponding to the lowest total pressure condition, and hence the highest ionization degree, as expected. Table 2 provides the summary of the results, reporting time average values of the pressure with and without MHD interaction, the pressure increases, the pressure coefficient with and without MHD interaction, and its increase at the three flow conditions considered in this experiment. Pressure increase and pressure coefficient increase have been, respectively, defined as

$$\Delta p = 100 \times \frac{p_{\text{mhd}} - p_{\text{nm}}}{p_{\text{nm}}} \tag{6}$$

Table 2 Time averages of the pressure measurements

Condition	Pressure in nonmagnetic runs, mbar	Pressure in MHD interaction runs, mbar	Pressure increase, %	Pressure coefficient in nonmagnetic runs	Pressure coefficient in MHD interaction runs	Pressure coefficient increase, %	V 1–4 Hall voltage, V
1	8.54	9.71	13.70	0.3196	0.3470	8.57	26.11
2	8.94	10.01	11.97	0.3102	0.3392	9.35	NA
3	10.79	11.57	7.23	0.3165	0.3350	5.85	20.01

$$\Delta Cp = 100 \times \frac{Cp_{\text{mhd}} - Cp_{\text{nm}}}{Cp_{\text{nm}}}$$
$$= 100 \times \left(\frac{p_{\text{mhd}} - p_\infty}{\rho_\infty u_\infty^2/2} - \frac{p_{\text{nm}} - p_\infty}{\rho_\infty u_\infty^2/2} \right) \Big/ \left(\frac{p_{\text{nm}} - p_\infty}{\rho_\infty u_\infty^2/2} \right)$$
$$= 100 \times \frac{p_{\text{mhd}} - p_{\text{nm}}}{p_{\text{nm}} - p_\infty} \tag{7}$$

An increase between roughly 5 and 13% is observed for what concerns surface pressure that corresponds to an increase between 5 and 9% on pressure coefficients; interestingly, even if the pressure increase at low density is higher, the influence on the Cp seems to stabilize around 9%. Additional tests at slightly higher pressure level (890 mbar) seem to confirm this trend with an increase of average pressure of about 1.8% and Cp of 2.2%.

C. Imaging

In Figs. 14 and 15 the argon flow in condition 3 around the test body is shown, with and without the MHD interaction. The two pictures have been taken with an exposure time of 1 ms and have been treated by means of the same logarithm stretching. The picture shown in Fig. 16 is taken with a 0.5 ms exposure time and depicts the MHD interaction in the same test condition. Being less saturated, the last picture allows one to better estimate the flow structure around the cone. Most notably, four bright rings can be seen around the cone in correspondence of the regions where the magnetic flux density is perpendicular to the flowfield, as an evidence of MHD action.

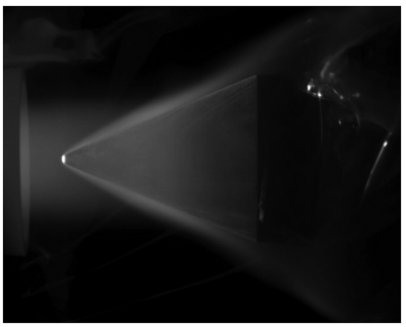

Fig. 14 Flow pattern without MHD interaction (exposure time: 1 ms).

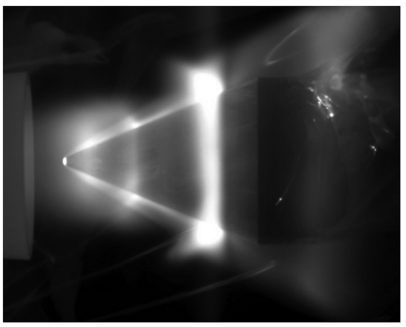

Fig. 15 MHD interaction around the magnetic cone (exposure time: 1 ms).

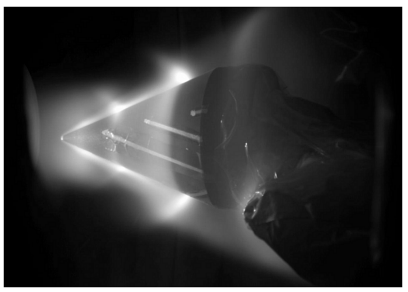

Fig. 16 MHD interaction around the magnetic cone (exposure time: 0.5 ms).

D. Electric Measurements

Electric voltage had been measured by means of the probes shown in Fig. 6 for conditions 1 and 3. The probe near the cone vertex is used as a reference probe. At both flow conditions, fluctuations smaller than 30% of the voltage have been observed, mainly produced by the electrical power supply system of an arc heater. In Fig. 17 the time behaviors of the voltages measured during MHD interaction experiments at flow condition 1 are shown. The plots of Fig. 18 are the time behaviors of the potential differences at flow condition 3. In both figures, the lines labeled V 1–2, V 1–3, and V 1–4 indicate the voltage between the reference probe 1 and the second, the third, and the fifth probes, respectively, along the cone surface starting from the cone vertex (see Fig. 6).

As can be noted, the voltage increases in the downstream probes as a result of an electric field directed against the argon flow. This result is in agreement with the qualitative calculation shown in Sec. III, where Eq. (4) gives the expression of the Hall electric field. From the

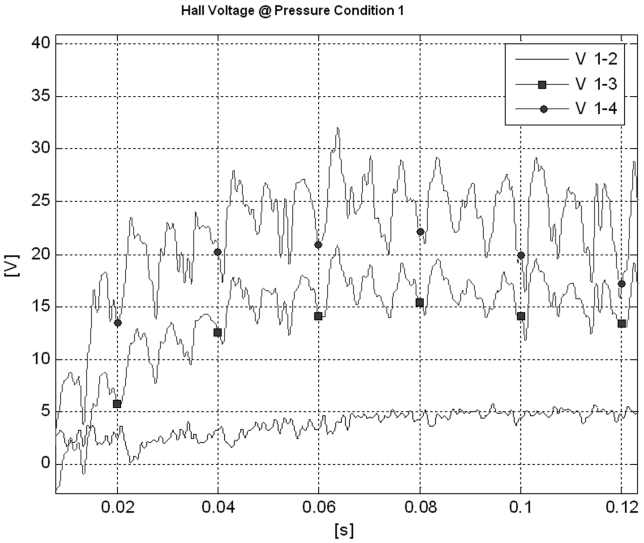

Fig. 17 Hall voltage distribution along the conical surface of the test body at flow condition 1.

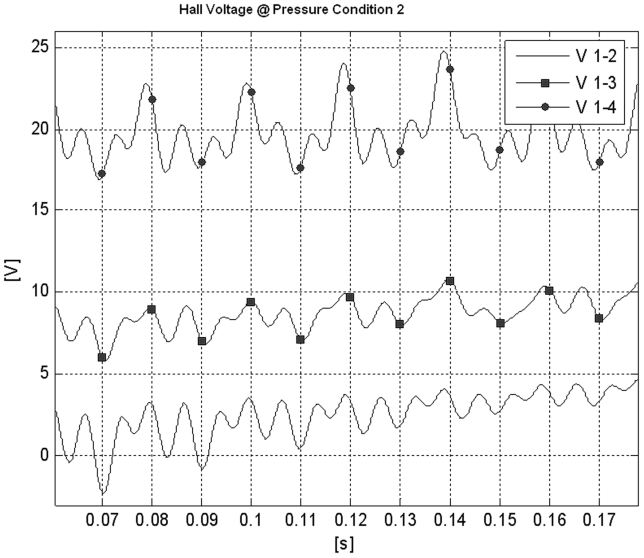

Fig. 18 Hall voltage distribution along the conical surface of the test body at flow condition 3.

measurement in condition 1, a value of about 500 V/m can be approximately estimated for the Hall field. In the last column of Table 2, the mean value of the V 1–4 voltage has been reported. As expected, in the low pressure condition, and, thus, at higher electron mobility, the Hall field is considerably higher than in the high pressure case.

V. Conclusions

The MHD interaction in a hypersonic flow was experimentally investigated. A conical test body had been placed at the exit of the hypersonic nozzle yielding an argon flow at a Mach number of 6. The test body incorporates an array of three permanent magnets producing the magnetic flux density necessary for the MHD interaction. This configuration appears to be well suited for high Hall parameter plasmas. The proposed configuration allows shorting the Faraday field inside the plasma along the azimuthal direction, enhancing the effect of the MHD interaction. Pressure, imaging, and electrical observations were done.

Experiments have been carried out in three test conditions, with different freestream pressure. In all the conditions considered, the measurements have shown significant effects of the MHD interaction. Images around the test body showed a rather different flowfield in the tests with and without MHD interaction. Bright rings appear in the region where the MHD interaction takes place.

Pressure measurements revealed that MHD interaction causes an increase of the pressure on the test body surface. The pressure increase in the presented experiment ranges between 6 and 13%, respectively, for the higher and lower pressure conditions. This is because, at low pressure, the ionization degree is higher and electrons exhibit a higher mobility, producing a higher conductivity and a higher plasma electrical current.

The Hall voltage was measured by means of electrical probes placed along the test body. Measurements demonstrate that a Hall field, directed against the flow, arises. The Hall voltage is higher in the low pressure test conditions. This, again, can be explained because of the higher electron mobility which, at lower pressure, produces higher Hall parameters. The results obtained are in qualitative agreement with the simplified model proposed in this paper.

The future developments of this activity include the realization of a new smaller sharp model that will allow the measurement of the surface temperature and heat flux. This kind of diagnostics is strongly affected by the plasma surrounding it and will therefore need a dedicated electronics setup. At the same time, it requires bigger sensors with respect to the pressure ones in order to reach the same ruggedness, complicating the mechanical placement of the sensor in the small test body. The feasibility of the use of nonintrusive diagnostics will also be addressed, to overcome the limitation of measurement points due to the insertion of sensors in the test body; for the concerns of the heat flux retrieval, the technique considered will be the one based on infrared thermography.

Acknowledgments

This work has been under the support of the European Space Agency (ESA) under the "Validation and Developments of Integrated Plasma and Fluid Dynamics Solvers" (PS-Just) Contract No. 18732. We would like to thank J. M. Muylaert for his support. We also would like to express our sincere gratitude to M. R. Carraro and Leonardo Biagioni for their help.

References

[1] Borghi, C. A., and Ishikawa, M., "New Concepts of MHD Power Generation" (invited paper), *12th International Conference on MHD Electrical Power Generation*, International Liaison Group on MHD Electric Power Generation (ILG-MHD), Moscow, Oct. 1996, Vol. 1, pp. 38–46.

[2] Gurianov, E. P., and Harsha, P. T., "AJAX: New Directions in Hypersonic Technology," AIAA Paper 96-4609, 1996.

[3] Bityurin, V. A., Lineberry, J. T., Potebnia, V. G., Alferov, V. I., Kuranov, A. L., and Sheikin, E. G., "Assessment of Hypersonic MHD Concepts," AIAA Paper 97-2393, 1997.

[4] Macheret, S. O., Shneider, M. N., and Miles, R. B., "MHD Power Extraction from Cold Hypersonic Air Flow with External Ionization," AIAA Paper 99-4800, 1999.

[5] Lineberry, J. T., Rosa, R. J., Bityurin, V. A., Botcharov, A. N., and Potebnya, V. G., "Prospects for MHD Flow Control for Hypersonics," AIAA Paper 2000-3057, 2000.

[6] Litchford, R. J., Cole, J. W., Lineberry, J. T., Chapman, J. N., Schmidt, H. J., and Lineberry, C. W., "Magnetohydrodynamic Augmented Propulsion Experiment: 1. Performance Analysis and Design," AIAA Paper 2002-2184, May 2002.

[7] Moorhouse, D. J., and Suchomel, C. F., "Exergy Methods Applied to Hypersonic Vehicle Challange," AIAA Paper 2001-3063, 2001.

[8] Golovachov, Y., Kurakin, Y., Schmidt, A., and Van Wie, D., "Numerical Simulation of 3D MHD Flow in a Duct Modeling a Hypersonic Intake," AIAA Paper 2003-171, 2003.

[9] D'Ambrosio, D., and Pandolfi, M., "An Upwind Numerical Method for the Prediction of Ideal MHD High Speed Flows," AIAA Paper 2004-2164, June 2004.

[10] Shang, J. S., Surzhikov, S. T., Kimmel, R., Gaitonde, D., Menart, J., and Hayes, J., "Mechanisms of Plasma Actuators for Hypersonic Flow Control," *Progress in Aerospace Sciences*, Vol. 41, No. 8, 2005, pp. 642, 668.

[11] MacCormack, R. W., "Simulation of Hypersonic Flow About an Air Vehicle with Strong Magnetic Field Interaction," AIAA Paper 2006-3232, June 2006.

[12] Ziemer, R. W., "Experimental Investigation in Magneto-Aerodynamics," *American Rocket Society Journal*, Vol. 29, No. 9, 1959, pp. 642–647.

[13] Shang, J. S., Kimmel, R., Hayes, J., Charles Tyler, and Menart, J., "Hypersonic Experimental Facility for Magnetoaerodynamic Interactions," *Journal of Spacecraft and Rockets*, Vol. 42, No. 5, 2005, pp. 780–789.

[14] Bobashev, S. V., Erofeev, A. V., Lapushkina, T. A., Poniaev, S. A., Vasil'eva, R. V., and Van Wie, D. M., "Effect of Magnetohydrodynamics Interaction in Various Parts of Diffuser on Inlet Shocks: Experiment," *Journal of Propulsion and Power*, Vol. 21, No. 5, 2005, pp. 831–837.

[15] Bityurin, V., Bocharov, A., and Lineberry, J., "MHD Flow Control in Hypersonic Flight," AIAA Paper 2005-3225, 2005.

[16] Matsuda, A., Wakatsuki, K., Takizawa, Y., Kawamura, M., Otsu, H., Konigorski, D., Sato, S., and Abe, T., "Shock Layer Enhancement by Electro-Magnetic Effect for Spherical Blunt Body," AIAA Paper 2006-3573, June 2006.

[17] Borghi, C. A., Carraro, M. R., Cristofolini, A., Bagatin, M., Veefkind, A., and Biagioni, L., "Experimental Investigation on the Magneto-Hydrodynamic Interaction in the Shock Layer on a Hypersonic Body," AIAA Paper 2004-2265, 2004.

[18] Borghi, C. A., Carraro, M. R., and Cristofolini, A., "An Axi-Symmetric Hall Configuration for the MHD Interaction in Hypersonic Flows," AIAA Paper 2005-4785, 2005.

[19] Scortecci, F., Paganucci, F., d'Agostino, L., and Andrenucci, M., "A New Hypersonic High Enthalpy Wind Tunnel," AIAA Paper 97-3017, July 1997.

[20] Scortecci, F., Paganucci, F., and d'Agostino, L., "Experimental Investigation of Shock-Wave/Boundary-Layer Interactions Over an Artificially Heated Model in Hypersonic Flow," AIAA Paper 98-1571, April 1998.

[21] Borghi, C. A., Carraro, M. R., Cristofolini, A., Gorse, C., Colonna, G., Passaro, A., and Paganucci, F., "Non-Intrusive Characterization of the Ionized Flow Produced by an Hypersonic Nozzle for MHD Interaction Experiments," AIAA Paper 2006-8050, 2006.

[22] Colonna G., and Capitelli M., "Self-Consistent Model of Chemical, Vibrational, Electron Kinetics in Nozzle Expansion," *Journal of Thermophysics and Heat Transfer*, Vol. 15, No. 3, 2001, pp. 308–316.

[23] Mitchner, M., and Kruger, C. H., *Partially Ionized Gases*, Wiley-Interscience, New York, 1973.

I. Boyd
Associate Editor